Journal of Cardiovascular Magnetic Resonance, 1(1), 59–64 (1999)

INVITED PAPER

Use of MRI in ASD Asessment

A Magnetic Resonance Imaging Method for Evaluating Atrial Septal Defects

Godtfred Holmvang

Cardiac Unit and the Department of Radiology, Massachusetts General Hospital, Harvard Medical School, and the Boston Heart Foundation, Cambridge, Massachusetts

Excellent definition of anatomic structure, ability to provide detailed flow information, and a global field of view make magnetic resonance imaging (MRI) well suited as a tool for the noninvasivè diagnosis of congenital heart disease. One of the most frequently encountered lesions is the atrial septal defect (ASD), which may be associated with important morbidity in the long term if unrecognized. The need for correction of the defect is most often defined by the magnitude of the trans-septal shunt flow. Increasingly, the evaluation also includes an assessment of the suitability of the lesion for percutaneous closure by new catheter-based techniques. This requires detailed knowledge of the size and location of the defect and of its proximity to other structures, such as the atrioventricular valves, the venae cavae, and the pulmonary veins.

By far the most common form of ASD is the secundum type in which the defect is located at the fossa ovalis in the central part of the interatrial septum. Lesions in this region may be difficult to evaluate by MRI because of marked thinning of the normal septum (Fig. 1). The defect may involve only part of this thin membrane that is not imaged reliably by standard T1 spin-echo techniques because of its relatively low signal intensity and very narrow profile, particularly if the course of the septum through the slice thickness is somewhat oblique. These factors often result in signal "dropout" at the fossa ovalis, creating the appearance of an ASD, even when the septum is intact.

The presence of a defect can be established definitively by using bright blood cine techniques to identify the ASD jet across the septum (1). Visualization of the shunt flow as an area of low signal in the right atrium is not always reliable, however. The definition of such a flow-related signal void can be improved by applying a spatial saturation slab to spins in the inflow region to the ASD (2). A defect diameter is established by the width of the trans-septal flow stream at its base, but multiple parallel or intersecting cine slices through the ASD may be required to define the ASD completely, including its maximum dimension.

An alternative approach for defining the major and minor diameters of an ASD and its shape is to view the defect "en face" by acquiring a phase contrast cine at a slice location that precisely matches the plane of the defect. The ASD is then defined by flow-related signal enhancement or phase changes in cine images of the cross-section of the trans-septal flow stream, as the flow is shaped by the orifice.

This en face imaging plane requires localizer acquisitions in two orthogonal views for accurate orientation in three dimensions. Using the image from the four-chamber view in which the defect in the atrial septum is seen most clearly [Fig. 2(A)], a modified short-axis view is prescribed such that the short-axis slices will be orthogonal to a line connecting the defect edges in the four-chamber view [Fig. 2(B)]. With prior knowledge of the

Received April 1998; Accepted April 1998
Address reprint requests to G. Holmvang.

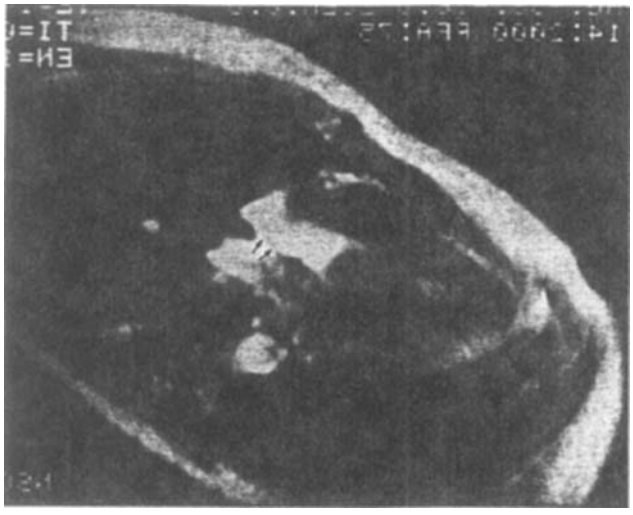

Figure 1. Gradient-echo cine frame in a four-chamber view demonstrating the thin membrane (at arrows, which are located in the left atrium) covering the fossa ovalis between the thicker parts of the interatrial septum at either end. The membrane is profiled by bright blood in the atrial chambers and is bowing toward the right atrium. The septum is intact; there is no signal void in the right atrium from trans-septal flow. A secundum ASD, when present, may involve only part of this thin membrane.

timing of the slices in the cardiac cycle, the acquisition is planned so that the short-axis slice through the center of the ASD is obtained near end systole or in the early diastolic rapid-filling period (approximately 400 msec after the R wave). This is the time of peak flow through the ASD and therefore also the optimal time for imaging the trans-septal flow stream. By anticipating this timing, a short-axis image centered in the ASD is obtained [Fig. 2(C)], from which the en face cine imaging plane can be prescribed precisely at the location of the defect at the time of peak flow. This cine slice in the plane of the septum at the ASD is sandwiched between two additional cine imaging planes that bracket the ASD orifice, with no gap between the slices [Fig. 2(D)].

The stack of three cine acquisitions produces cross-sections of the ASD flow stream at different levels with respect to the orifice. The flow at each level tends to have a characteristic appearance, although this can be somewhat variable. On the left atrial side there is usually increased signal intensity in the flow convergence zone immediately proximal to the ASD; this region of signal enhancement is usually slightly smaller than the full extent of the defect [Fig. 3(A)]. The flow is stable, and no signal void develops. At the orifice [Fig. 3(B)], a narrow signal void frequently appears at the periphery of the flow stream (which again tends to be relatively bright); this low signal intensity rim is attributed to shear effect or local disturbed flow at the edges of the defect, and the signal void is included in measurements of the defect diameter. Cross-sections of the shunt flow downstream from the orifice most often show a variable signal void corresponding to complex flow in the jet [Fig. 3(C)]. The signal attenuation can range from minimal to complete, presumably depending on how restrictive the orifice is and on the resulting interatrial pressure gradient. The low signal area may be somewhat larger than the actual defect and tends to develop indistinct borders as the jet expands in the right atrium.

Based on a review of the cine loops, the frames with the best localization at the orifice and with timing that gives the best definition of the shunt flow are selected for measurement. Very frequently the flow boundaries along the defect edges are seen more completely and more sharply in phase velocity maps reconstructed from the cine data that are acquired with velocity encoding in the slice-selection direction [Fig. 3(D)].

ASD shape and diameter determined from such cine images in the plane of the ASD have been validated (3). An advantage of these en face images is that the measured dimensions are more accurate than those derived from standard spin-echo images, which tend to overestimate substantially both the diameter and area of secundum ASDs. This is presumably due to signal dropout at the fossa ovalis in areas where there is thinning of the intact septum adjacent to the defect; this would make the defect appear larger than it is.

An additional advantage of the en face images is that the maximal diameter can be defined without ambiguity. Figure 4(A) and (B) shows the flow area across a large ASD. The cross references mark the intersections of the defect with slices acquired in the four-chamber and short-axis views, respectively. Not one of these orthogonal images is aligned adequately with the major axis of the elliptical orifice, and an accurate measurement of the maximal defect diameter would therefore not be possible in the two standard views.

The cine images of the flow cross-section at the ASD also allow quantitation of the magnitude of the shunt from the very same images that define defect shape and dimensions. The phase velocity maps calculated from the cine data (velocity encoded in the through-plane direction) can be integrated over the ASD area and over time through the cardiac cycle to give the shunt volume per heart beat and hence per minute. Figure 5 shows the calculated volume flow rate across the ASD as a function

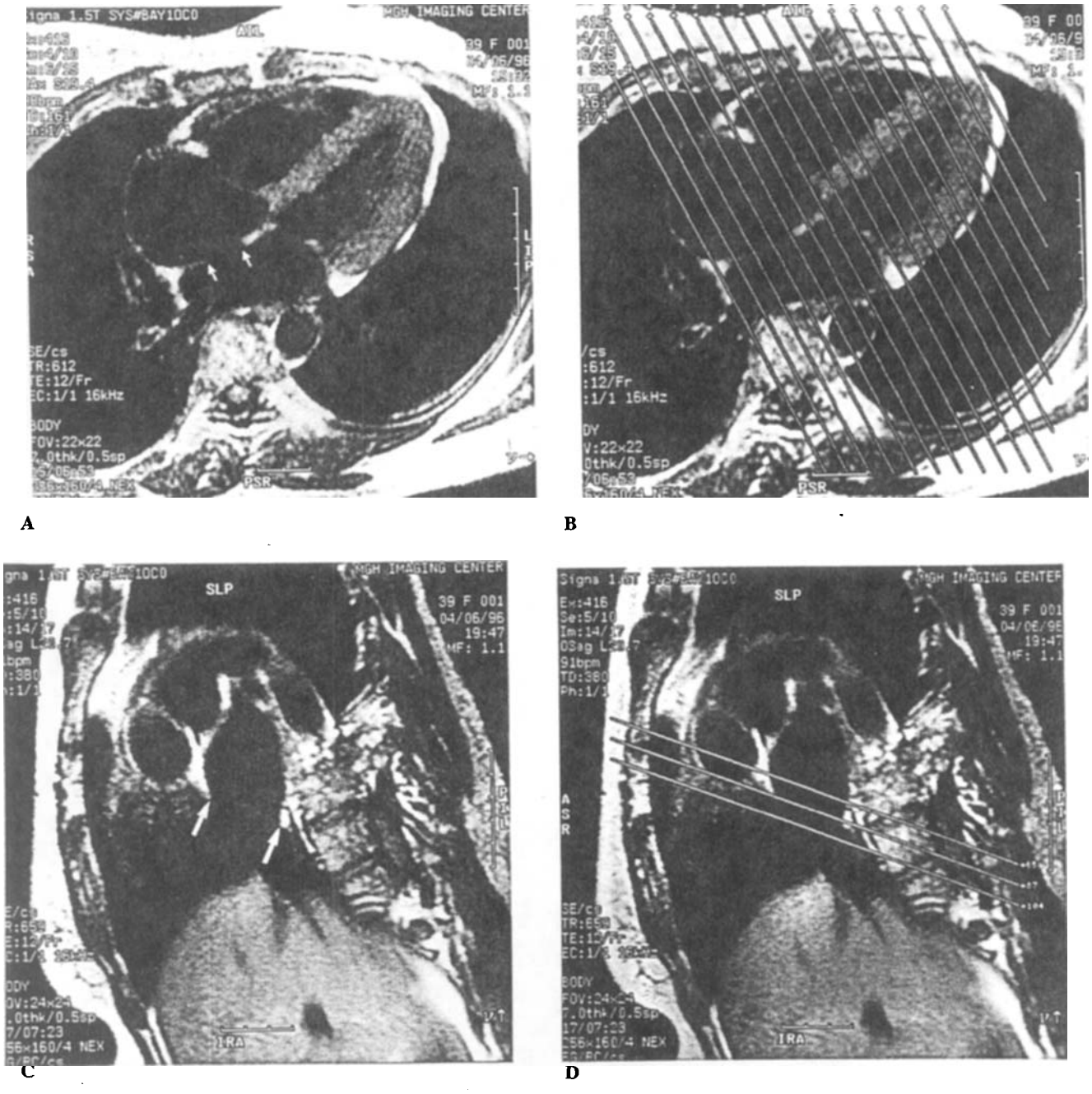

Figure 2. (A) T1 spin-echo image in four-chamber view showing a secundum ASD. The two arrows in the left atrium point to the apparent defect edges. (B) Graphic prescription of a modified short-axis view that will make the images orthogonal to a line connecting the defect edges in the four-chamber view [arrows in (A)]. The stack is adjusted so that the timing of the slice through the center of the ASD (slice 14) is approximately at end systole. (C) Modified short-axis view at the center of the secundum ASD in (A) [slice 14 from the prescription in (B)]. The timing in the cardiac cycle is 380 msec after the R wave (near end systole). The two arrows in the right atrium point to the apparent defect edges. (D) Graphic prescription of three contiguous phase contrast cine acquisitions bracketing the ASD orifice, with the center slice coincident with the plane of the defect.

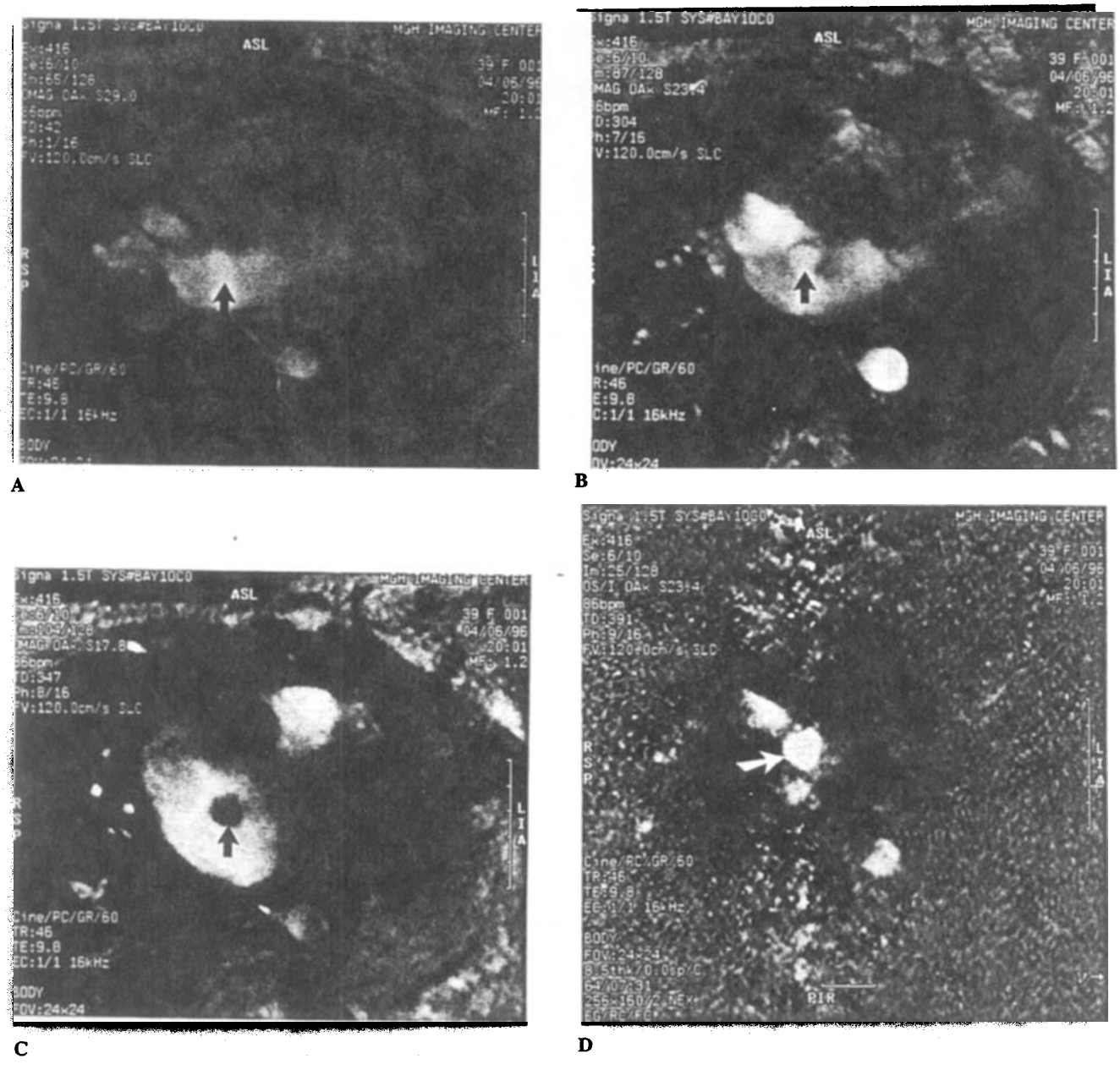

Figure 3. One frame from the phase contrast cine at each of the three levels prescribed in Fig. 2(D), showing adjacent cross-sections of the left-to-right trans-septal flow (black arrows) upstream in the left atrium (A), at the ASD (B), and downstream in the right atrium (C) at times in the cardiac cycle when this flow is well defined. The flip angle is relatively steep (60°) to emphasize flow-related enhancement effects. (D) Phase velocity map (velocity encoding 120 cm/sec) from the middle slice [at the level of (B)] centered at the ASD orifice, in which the defect border is defined by the outer edge of the bright (high velocity) region of trans-septal flow (white arrow), so that slower velocities at the periphery of the flow are included. The maximal diameter in this case is 16 mm. For description of additional details, see text.

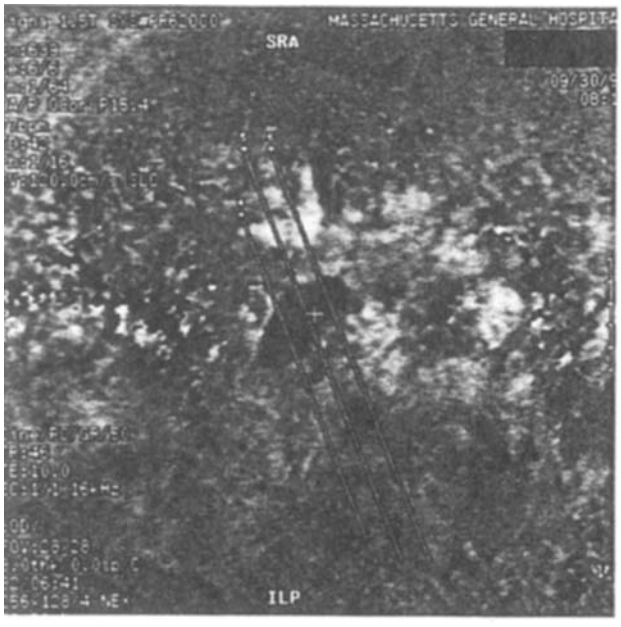

A

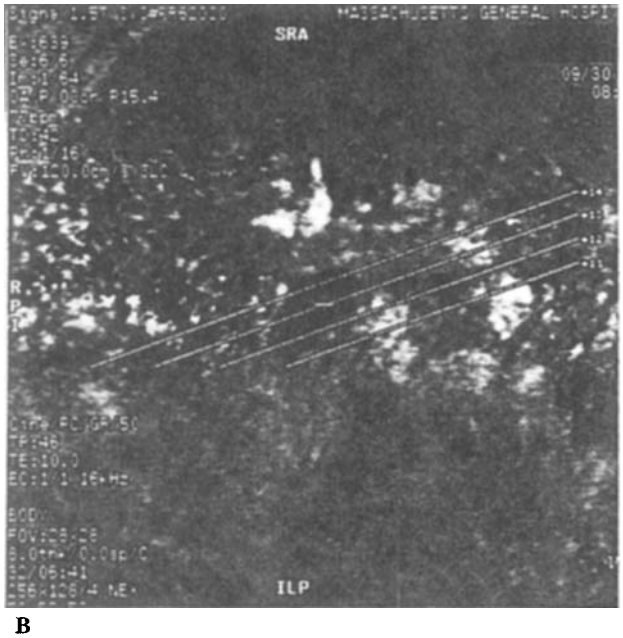

B

Figure 4. En face view of a different ASD (black region at center of image) with cross-references showing intersections with slice locations in the standard four-chamber (A) and short-axis (B) views. None of these standard slices capture the long axis of this elliptical orifice.

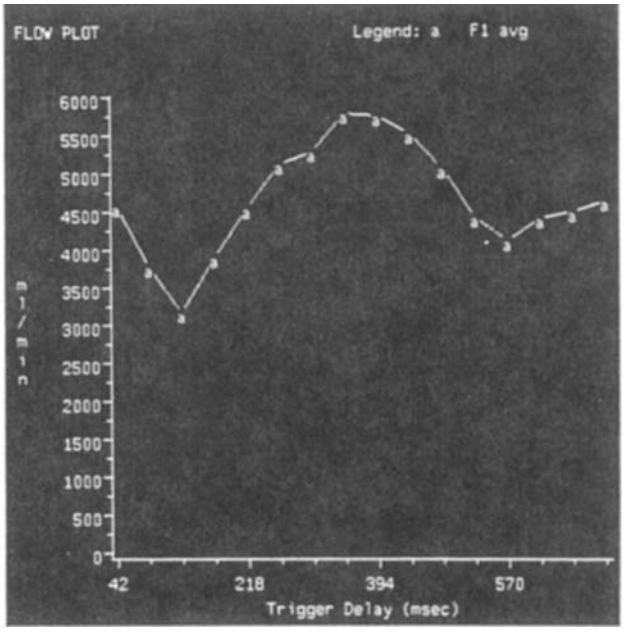

Figure 5. Volume flow rate across the ASD as a function of time for the lesion shown in Figs. 2 and 3 calculated from phase velocity maps obtained from the cine acquisition in the plane of the defect [Fig. 3(D)] by integrating the flow velocity over the orifice area at each of 16 time points through the cardiac cycle. For quantitation of the shunt, see text.

of time in the patient whose images appear in Figs. 2 and 3. The shunt volume is 4660 ml/min, which compares with a cardiac output of 5142 ml/min measured by the same technique in an axial view of the ascending aorta. The pulmonary-to-systemic flow ratio is therefore 1.9:1 (ignoring coronary flow in this case).

Successful imaging of secundum ASDs in the en face view depends on the presence of trans-septal flow, and the method would not be expected to demonstrate patent foramen ovales reliably; these may permit trans-septal flow only briefly during maneuvers such as coughing or Valsalva. Another limitation is that the method may perform suboptimally with complex ASDs in which a "flap" deflects the flow stream away from a course perpendicular to the septum (i.e., to the cine imaging plane). Such defects may be better evaluated in an orthogonal view such as the four-chamber view.

In summary, phase contrast cine imaging of the cross-section of the trans-septal flow at the orifice results in an en face view of ASDs that permits comprehensive and efficient evaluation of the defect, with quantitation of the

shunt volume in addition to defining shape and dimensions with improved accuracy compared with views that show the interatrial septum in profile.

REFERENCES

1. Theissen P, Sechtem U, Mennicken U, Hilger HH and Schicha H. Noninvasive diagnosis of atrial septal defects and anomalous pulmonary venous return by magnetic resonance imaging. *Nuklearmedizin,* 1989; 28:172–180.
2. Hartnell GG, Sassower M and Finn JP. Selective presaturation magnetic resonance angiography: New method for detecting intracardiac shunts. *Am Heart J,* 1993; 126:1032–1034.
3. Holmvang G, Palacios IF, Vlahakes GJ, Dinsmore RE, Miller SW, Liberthson RR, Block PC, Ballen B, Brady TJ and Kantor HL. Imaging and sizing of atrial septal defects by magnetic resonance. *Circulation,* 1995; 92:3473–3480.